Scientia Iranica A (2015) 22(4), 1390–1401

SCIENTIA IRANICA

Sharif University of Technology
Scientia Iranica
Transactions A: Civil Engineering
www.scientiairanica.com

Flexural behaviour of notched steel beams repaired with FRP plates: Parametric studies

M. Motaleb and M.Z. Kabir*

Department of Civil and Environmental Engineering, Amirkabir University of Technology, Tehran, P.O. Box 15875-4413, Iran.

Received 27 October 2013; received in revised form 22 September 2014; accepted 27 October 2014

KEYWORDS
FE;
Repair;
Steel beams;
Notch;
FRP plate;
Parametric study.

Abstract. The load carrying capacity in a damaged steel beam can be substantially increased through repairing by attaching Fiber-Reinforced-Polymer (FRP) plates to tension flange. Such a repaired beam is generally failed by either debonding of the FRP plates from the steel flange or FRP rupture at the damage location due to the stress concentration. In this case, the effectiveness of repair significantly depends on the repairing material properties, i.e. FRP and adhesive. This paper developed a Finite Element (FE) modeling of damaged steel beams repaired with FRP plates, and aimed to clarify the FRP and adhesive properties effects on beam recovery. The primary defect was simulated by inserting a notch through the tension flange at mid-span. To ensure the validity of the proposed numerical model, the results of numerical models were compared with those existing experimental works. A parametric study was performed to achieve a better understanding on the sensitivity of parameters which are responsible for flexural behavior of the repaired beams. Studies showed that the influence of the most investigated parameters on the response of the repaired beam is very notable, and considering influential parameters in choosing the material for a FRP-repair leads to promising results in design consideration.

1. Introduction

In practice, steel beams are vulnerable to be exposed to various factors through which their capacity is decreased such as fatigue crack, physical damage, corrosion, wrong cutting during construction, and so on. Carbon Fiber Reinforced Polymer (CFRP) composites as construction materials are being increasingly considered for repairing and strengthening the existing structures because of their key advantages, including high strength-to-weight ratio, corrosion resistance, light weight and high durability.

Even though the efficiency of the bonded CFRP for the strengthening and repair of steel structures has been presented in a number of studies [1-13], it can be seen that the technique is not yet as extensive as it is for the concrete members. Up to now, most of the previous studies focused on the behavior of the strengthening effect of FRP on undamaged steel beams. However, in some experimental studies, the influence of CFRP plates on the strength of artificially damaged steel beams has been investigated. In the experiments conducted by Tavakkolizadeh and Saadatmanesh [13], the ultimate load-carrying capacities of damaged girders in which damage varied from 25% loss of the flange to 100%, significantly increased by 80% compared to the intact beam. Liu and et al. [12] reported that an increase in stiffness and plastic load of corroded steel members can be achieved from the application of CFRP laminates to the tension flange of corroded steel members. In another experimental study [5,9], it was resulted that attaching CFRP plate to tension flange of a notched steel beam increased its load carrying capacity up

*. *Corresponding author. Tel.: +98 21 64543016; Fax: +98 21 66414213*
E-mail address: mzkabir@aut.ac.ir (M.Z. Kabir)

to 79% of that for the intact beam. According to another experimental study conducted by Harries and et al. [7], the externally bonded CFRP plates increased the load required to cause yield at the root of the notch to 137% of that of the unrepaired beam. Also, in the other detailed aspect of repairing the metallic members, some researchers have worked on finding an efficient patch repair which is very important from both economic and technical point of view [14-17].

However, the limited knowledge of behavior in such applications needs to be extended. The lack of knowledge about interaction between the behavior of the damaged beam and the properties of repairing materials (i.e., mechanical and dimensional properties of FRP and adhesive layer) are some of the problems contributing to the difficulty of having a clear view toward FRP-repair.

The aim of this paper is to recognize the contribution of each physical and mechanical parameter of materials to behavior of repaired beams under monotonic loading. In this direction, a validated numerical modeling was developed, approaching by incorporating causal factors in the behavior of beams. It was assumed that a beam suffered from an initial notch passed through its tension flange, and attaching FRP plates to notched flange was implemented to recover the beam behavior. In order to simulate the damaged steel beam, a notch was cut through its tension flange at mid-span. The notch was inserted to reflect the reduction in the elastic stiffness and the ultimate strength of the beam. In order to validating the FE results, various beams tested by other researchers were simulated to compare the results.

2. Finite element model

The simply supported beams were modeled using the FE program ABAQUS version 6.10 [18] to simulate the mechanical behavior of the repaired beams. To reduce the time consuming in analysis process, only half of the steel beam were modeled in which necessary constraints were assigned to nodes of the symmetric surface, as shown in Figure 1.

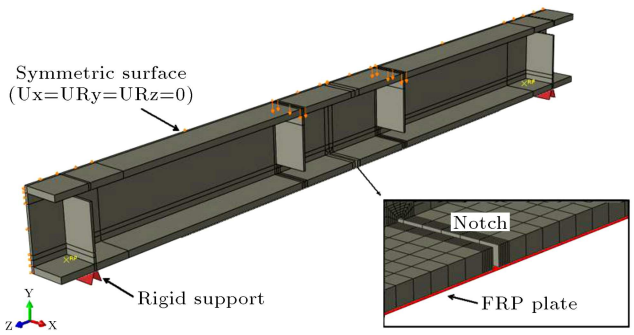

Figure 1. Model configuration.

2.1. Information about modeling and elements

The present study simulated the nonlinear mechanical behavior of the repaired steel beam subjected to four points loading. The initial damage in a steel beam was modeled by geometrical cut extrusion in the bottom flange at the mid-span. The FE model consists of three parts: steel, adhesive and FRP as shown in Figure 1. For FRP and steel beams, four-node shell elements with reduced integration, S4R, were adopted. Cohesive behavior, as a feature of ABAQUS version 6.10, which is suitable for modeling the behavior of adhesive joints [18], was used to model the adhesive layer (explained in Section 2.4.2). Figure 1 shows the model configuration as well as the inserted notch in which a half circle cutting above the notch was modeled to overcome convergences problems. It should be noted that to have a better view, shell thickness with the scale of unit is shown in Figure 1.

2.2. Boundary conditions and load application

Displacement-type boundary condition was used to apply the external loading to the beam. Two rigid surfaces as supports were defined and individual reference points were assigned to each of them, as shown in Figure 1. Fixing the degrees of freedom at reference points, the constraints were applied to the entire rigid part and the reaction force transmitted to the reference point. In addition to satisfying simple support conditions, this approach enables us to record the exact amount of the reaction force throughout the loading.

2.3. Constraints and contact interactions

The steel beam-support plate and steel beam-composite plate interfaces were modeled by surface-to-surface contact interaction type, describing a contact between two deformable surfaces or between a deformable surface and a rigid surface. A friction model was used to define the resisting against tangential motion of the surfaces in a mechanical contact analysis. The penalty friction formulation was selected to define the friction coefficients for steel-support.

2.4. Materials modeling

2.4.1. Steel

In this study, steel member was taken into account as an elastic-plastic material with strain hardening. A typical trilinear stress-strain diagram of steel is shown in Figure 2. The model was developed based on the Mises yield surface, defined by giving the value of the uniaxial yield stress as a function of uniaxial equivalent plastic strain [19]. Also, the isotropic hardening model was used to define the strain hardening of materials.

2.4.2. FRP composite material

As mentioned earlier, CFRP plates were modeled using shell elements. Composite layup was employed to specify the thickness, the number of integration points,

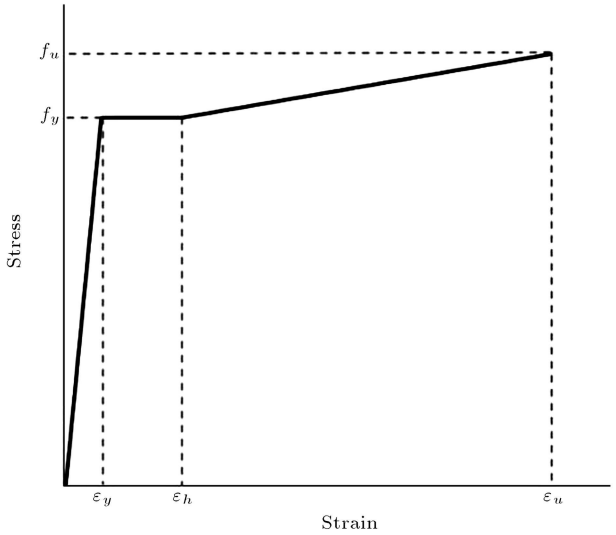

Figure 2. Idealized stress-strain relationship for steel.

the material, and the orientation for each layer of the shell. The integration method is Simpson's rule with three points in each layer for a composite section.

The CFRP materials were assumed to behave in a linearly elastic manner without showing any plasticity behavior. However, the damage initiation occurred after satisfying one of the plane stress failure criteria which was developed by Hashin [20]. He introduced fiber and matrix failure criteria that distinguish between tension and compression failure. These criteria assume a quadratic interaction between the tractions acting on the plane of failure. Given the difficulty in obtaining the plane of fracture for the matrix compression mode, Hashin used a quadratic interaction between stress invariants [21] which is available in Abaqus package [18]:

Fiber tension mode:

$$\left(\frac{\sigma_{11}}{X^T}\right)^2 + \left(\frac{\sigma_{12}}{S^L}\right)^2 = 1, \quad \sigma_{11} > 0. \tag{1}$$

Fiber compressive mode:

$$\left(\frac{\sigma_{11}}{X^C}\right)^2 = 1, \quad \sigma_{11} < 0. \tag{2}$$

Matrix tension mode:

$$\left(\frac{\sigma_{22}}{Y^T}\right)^2 + \left(\frac{\sigma_{12}}{S^L}\right)^2 = 1, \quad \sigma_{22} > 0. \tag{3}$$

Matrix compressive mode:

$$\left(\frac{\sigma_{22}}{2S^T}\right)^2 + \left[\left(\frac{Y^C}{2S^T}\right)^2 - 1\right]\frac{\sigma_{11}}{Y^C} + \left(\frac{\sigma_{12}}{S^L}\right)^2 = 1, \quad \sigma_{22} < 0, \tag{4}$$

where σ_{ij} are components of the effective stress tensor in the directions 1 (fiber direction) and 2 (matrix direction). X^T, X^C, Y^T, Y^C, S^L and S^T denote the longitudinal tensile strength, the longitudinal compressive strength, the transverse tensile strength, the transverse compressive strength, the longitudinal shear strength and transverse shear strength, respectively.

Once the initiation criterion is satisfied, the damage evolution would describe the rate of degradation of the material stiffness up to the material failure. The evolution law is based on the energy dissipated through the damage process (see [22]).

2.4.3. Adhesive behavior

In the repaired steel beams, there are a number of failure modes including cohesive failure of the adhesive, debonding along the steel-adhesive or CFRP-adhesive interfaces which governs the strength of the bonded joint. Since a failure in interfaces is completely dependent on the surface preparation and manufacturing, the adhesive failure as a governing failure mode was merely taken into account. In this way, the surface-based cohesive behavior is defined as a surface interaction property to model the adhesive between FRP and steel beam. The formulae and laws governing this feature are very similar to those cohesive elements with traction-separation behavior [18]. Quadratic stress criterion, Eq. (5), was employed to show the damage initiation in which the damage will be initiated, when this equation satisfies [18]:

Quadratic stress criterion:

$$\left(\frac{\sigma_n}{\sigma_n^{\max}}\right)^2 + \left(\frac{\sigma_s}{\sigma_s^{\max}}\right)^2 + \left(\frac{\sigma_t}{\sigma_t^{\max}}\right) = 1, \tag{5}$$

where $\sigma_n^{\max}$, $\sigma_s^{\max}$, $\sigma_t^{\max}$, σ_n, σ_s and σ_t denote strength in normal direction, strength along the first shear direction, strength along the second shear direction, normal contact stress in the pure normal mode, shear contact stress along the first shear direction and shear contact stress along the second shear direction, respectively. Beyond the damage initiation point, a damage evolution based on energy was defined to describe the degradation of the cohesive stiffness.

It is recommended that surface-based cohesive behavior is better to use in situations where interfacial thickness is negligibly small, and interfacial stiffness is not in the first priority of the study [18]. Also, numerical investigation on shear strengthening of RC beams, conducted by Godat et al. [23] showed that changing the interfacial stiffness gives no effect on the overall structural performance, and the debonding point remains almost the same. Therefore, this feature of FE package, i.e. surface-based cohesive behavior, was adopted as a reliable option to show adhesive fail-

Table 1. Geometrical characteristics and details of repaired tested specimens.

No.	Beam set	Specimens	Type	Section type	Steel beam section	Damage level (% of the Flange's width)	CFRP modulus (GPa)	Area of CFRP (mm^2)	Length of FRP (% of the span)
1	Harries et al. [7]	A	Intact	Steel	W150×18	-	-	-	-
2		B	Unrepaired	Steel	W150×18	100	-	-	-
3		C	Repaired	Steel	W150×18	100	144	70	100
4	Fam et al. [5] and Howard [9]	Control	Intact	Steel	W100×19	-	-	-	-
5		FC1	Unrepaired	Steel	W100×19	100	-	-	-
6		HC1F1	Repaired	Steel	W100×19	50	201	167	88
7		FC1F1	Repaired	Steel	W100×19	100	201	334	88
8		FC1F2	Repaired	Steel	W100×19	100	396	204	88
9	Liu et al. [12]	U3	Repaired	Steel	W310×21	100	200	140	100
10		U4	Repaired	Steel	W310×21	100	200	140	12.5
11	Tavakkolizadeh and Saadatamnesh [13]	25%	Repaired	Steel-concrete	W355×13.6	25	144	193	83
12		100%	Repaired	Steel-concrete	W355×13.6	100	144	965	83

ure mode, as well as considering the slippage between FRP and steel surface.

3. Verification of the model

In order to validate the results obtained from the finite element models, a comparison between existing experimental results and the numerical predictions is conducted.

3.1. Simulated beams

12 specimens corresponding to the specimens tested by Harries et al. [7], Fam et al. [5], Howard [9], and Liu et al. [12], and two composite specimens tested by Tavakkolizadeh and Saadatmanesh [13] were adopted for numerical simulation. Table 1 summarizes the details of experimentally tested beams, and Figure 3 shows beam configuration as well as FE modeling of simulated beams. In these beams, various kinds of FRP plates have been utilized to attach to the bottom face of the notched tension flange. The simulated beams demonstrated the capability of properly modeling of the FRP-repair with a high accuracy for a wide variety of FRPs, as shown in Table 2 and Figure 4. Amounts of the ultimate load carrying capacities, initial stiffness and failure modes obtained through reported tested results and numerical analyses are summarized in Table 2. The greatest difference observed between experimental and numerical load carrying capacities was 9% for the simulated steel beam FC1F1 in which the beam eventually failed by rupturing in CFRP plate, while its corresponding beam in experimental study failed by complete debonding of CFRP from steel surface. It may come from the existing difference between adhesive properties adopted in numerical modeling and tested beams.

3.2. Failure modes

In order to calculate the load carrying capacity of the simulated beams, several failure modes were considered, including rupturing of the CFRP plate caused by breakage in fibers (R), complete debonding which means separation of whole FRP plate from steel beam (D), steel beam yielding in large area created in critical areas like crack location (Y), initiation of crack growth at the root of the notch due to stress concentration (CG), and local buckling in compressive flange or distortional one (B). It should be mentioned that in order to take the local buckling mode into account, whole beams were simulated rather than modeling only a portion of them.

4. Parametric study

Based on the validated model, a parametric study was conducted to gain better insight into the parameters governing the behavior of notched steel beams which are repaired with bonding a CFRP plate to bottom side of tensile flange. In this direction, the material properties and loading conditions were the same as those used in the experimental study on repairing the steel beam reported by Fam et al. [5] and Haward [9]. The steel beam was with W100 × 19 section, total span length of 900 mm, elastic modulus 200 GPa, and yield stress 398 MPa. High modulus CFRP plate, with 2 mm thickness covering 66% of the free span,

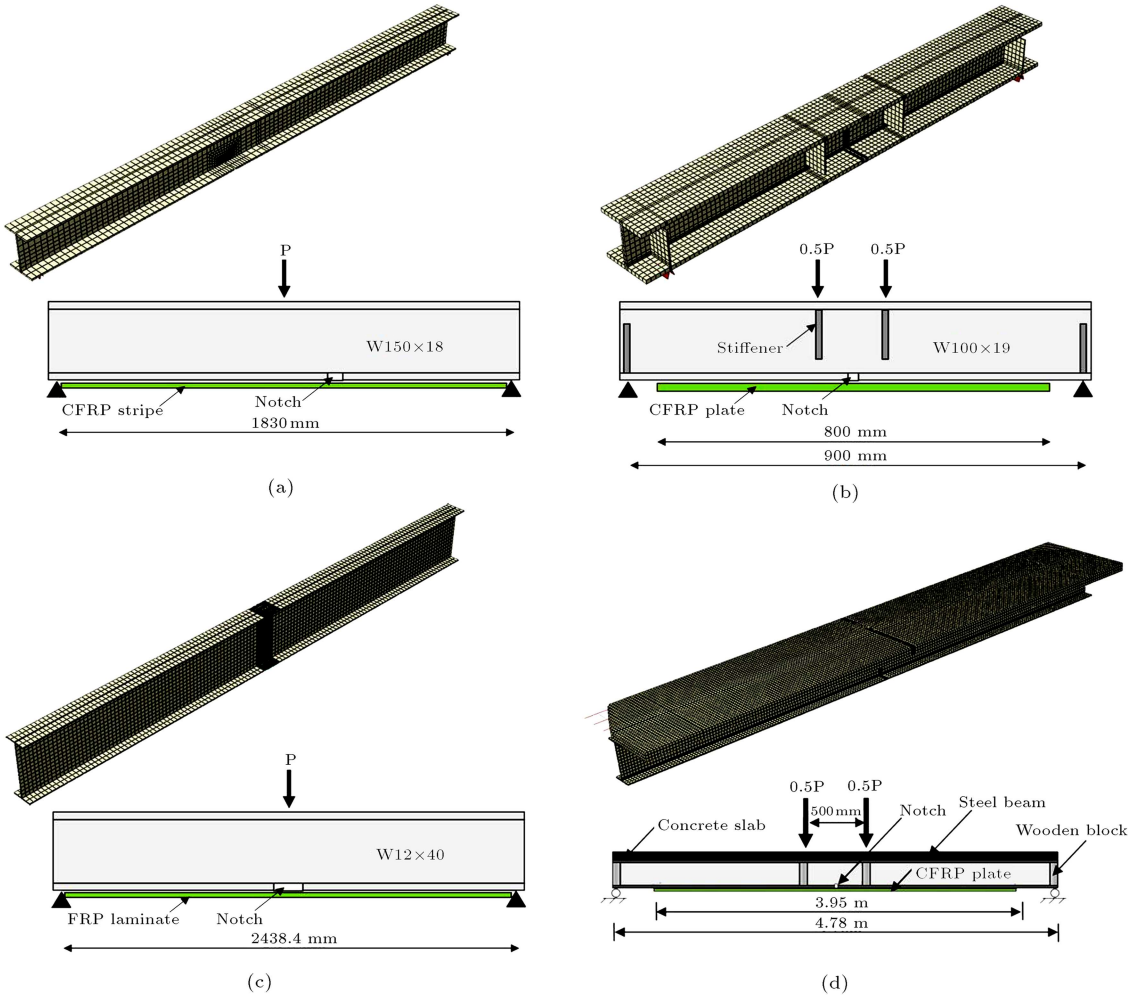

Figure 3. FE models and beam configuration of tested beams: (a) By Harries et al. [7]; (b) by Fam et al. [5]; (c) by Liu et al. [12]; and (d) by Tavakolizadeh and Saadatmanesh [13].

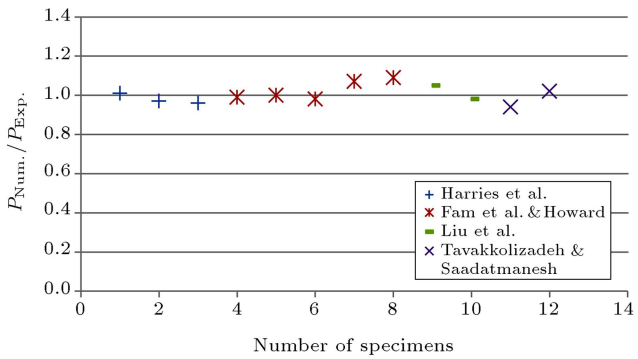

Figure 4. Accuracy of the numerical model over the experimental results.

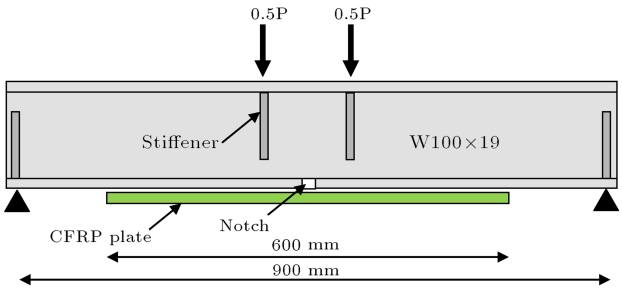

Figure 5. Schematic of loading setup and beam dimensions.

was used whose strength and modulus of elasticity was measured 1431 MPa and 396 GPa, respectively. In the experimental programs, two different notches with width of 1.3 mm and 3.3 mm were inserted into the tensile flanges. However, in this study, the notch with 3.3 mm width in tensile flange at mid span was merely considered to show initial damage. All specimens were loaded under a four-point bending; typical repair configuration along with the loading scheme is presented in Figure 5. In the following sections, when the effect of a specific parameter is analyzed, the values of all other parameters are kept constant.

4.1. Parameters related to FRP

4.1.1. Effect of tensile modulus of FRP laminate

To investigate the effect of FRP modulus on the behavior of the beam, the ultimate strength for FRP

Table 2. Comparison between experimental and numerical results.

No.	Beam set	Specimens	Type	Experimental results		Numerical results		$\frac{P_{Num}}{P_{Exp}}$	Failure modes[b]	
				Ultimate load	Elastic stiffness	Ultimate load	Elastic stiffness		Exp.	Num.
1	Harries et al. [7]	A	Intact	102.3	NR[a]	103.3	12.6	1.01	B	B-Y
2		B	Unrepaired	81.8	NR[a]	79	10.6	0.97	B	B-Y
3		C	Repaired	84.5	NR	80.7	10.9	0.96	B	B-Y
4	Fam et al. [5] and Howard [9]	Control	Intact	243	47.1	241.1	53.6	0.99	Y	Y
5		FC1	Unrepaired	101	36.1	95.35	38.7	0.94	Y-CG	Y-CG
6		HC1F1	Repaired	182	57	177.6	62.1	0.98	R	R
7		FC1F1	Repaired	105	55.6	112	59.1	1.07	R	R
8		FC1F2	Repaired	187	61.7	203.8	60.7	1.09	D	PD-R[c]
9	Liu et al. [12]	U3	Repaired	165.5	-	173.5	21.2	1.05	D	PD-Y[c]
10		U4	Repaired	149.5	-	147.2	20.1	0.98	D	D
11	Tavakkolizadeh and Saadatamnesh [13]	25%	Repaired	471.8	19.6	441.5	18.65	0.94	R	R
12		100%	Repaired	434	19.6	443.2	21.22	1.02	D	CG-PD

[a] Not reported.

[b] B: Buckling, Y: Yielding, CG: Crack Growth at root of the notch, R: Rupture of CFRP, PD: Partial Debonding, and D: complete Debonding.

[c] Differences between failure modes may be due to the difference between adhesive properties and also lack of surface preparation in tests.

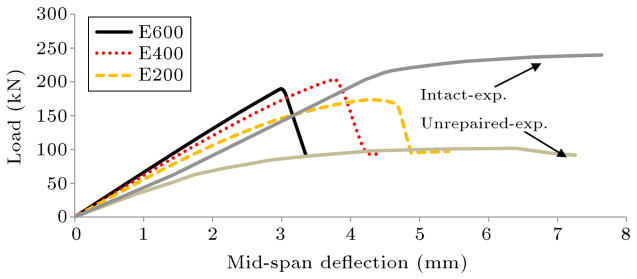

Figure 6. Load-deflection curve of repaired beams with various FRP modulus.

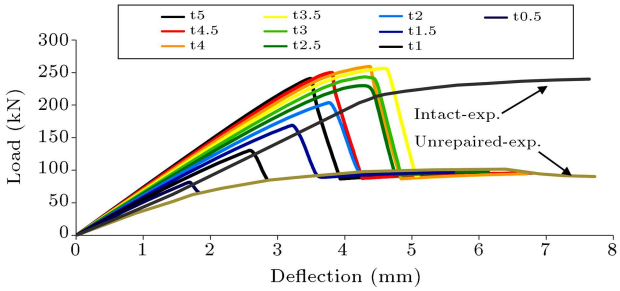

Figure 7. Load-deflection curve of repaired beams with various FRP thickness.

plate was assumed to be constant and three elastic moduli equal to 200 GPa, 400 GPa, and 600 GPa were taken into account. It is obvious that because of the linear behavior in FRP material and assuming ultimate strength to be constant, the ultimate strain of FRP is decreased while increasing the elastic modulus of FRP. As Figure 6 shows, the elastic modulus has a direct relation with elastic stiffness of the beams. Repair using FRP plates with Young's modulus of 200 GPa, 400 GPa, and 600 GPa improved elastic stiffness of damaged beams up to 45%, 60%, and 72%, respectively. Failure in the adhesive layer was observed as a predominant failure mode of repaired beam using E200, while repaired beams by both the E600 and E400 demonstrated almost a linear behavior until reaching the highest point, where beams failed by rupturing of CFRP plate. This diagram indicates that increasing in the modulus of elasticity without changing the ultimate strength of the CFRP plate, not only reflects any considerable improvement in the ultimate strength of the beam, but also makes beam to present a brittle failure in which load carrying capacity dramatically drops. In the case of the repaired beam with E600, for example, due to the reduction in the ultimate strain of the CFRP plate, CFRP fails at the lower load level compared to the repaired beam with E400.

4.1.2. Effect of FRP thickness

The second investigated parameter was the thickness of the FRP plate. Figure 7 shows the effect of the variation of the thickness of plate from 1 mm to 5 mm. This figure shows that by increasing the thickness of CFRP plate, the failure mode changes from fiber breakage to debonding mode. Beams, repaired with CFRP plates in which thickness varied between 1 mm to 2 mm eventually failed by occurring the rupture of

CFRP plate at the mid-span, while the thicker plates completely debonded from the surface of steel flange at the peak points. The distinction between rupturing and debonding can be seen in the descending parts of diagrams. Figure 7 shows that the repair with thickness of 2.5 mm almost restores the load carrying capacity of damaged beam into an intact one. As can be seen in Figure 7, increasing the thickness of CFRP plates from 2.5 mm to 4 mm led to strength growth of beams which finally dropped due to the fiber collapse. However, high thickness values of CFRP do not always lead to a higher gain in the load carrying capacity. Figure 7 clearly shows this phenomenon that when FRP thickness increases from 4 mm to 5 mm, any enhancement of beam strength is gained, and causes a reduction in the ultimate load carrying capacity to occur. The reason of this behavior will be discussed in Section 4.5.2.

4.1.3. Effect of type of FRP plate

Available FRP plates are of various types related to their characteristics such as ultimate strain which is associated with their modulus of elasticity. Therefore, in order to reveal the influence of FRP type on the repair-scheme, four commercially available FRP products with various elastic moduli, consisting of GFRP (Glass-FRP) plates with modulus of elasticity 31 GPa and ultimate strain 0.031, SM-CFRP (Standard Modulus) with modulus of elasticity 144 GPa and ultimate strain 0.0148, HM-CFRP (High Modulus) with modulus of elasticity 396 GPa and ultimate strain 0.00361, and UHM-CFRP (Ultra High Modulus) with modulus of elasticity 514 GPa and ultimate strain of 0.00332 were adopted. In this case, all of the dimensional properties of materials were assumed to be constant. Figure 8 shows the load-deflection responses for repaired beams in which UHM-CFRP plate enhances the strength of the beam by almost the intact one. It shows that increasing the elastic stiffness is associated with the elastic modulus of each type of CFRP. The contribution of CFRP and the effect of its elastic modulus on flexural stiffness are more pronounced after yielding steel in compressive flange and damaged area, compared to the elastic range. However, the flexural strength is not always in direct relation with ultimate strength

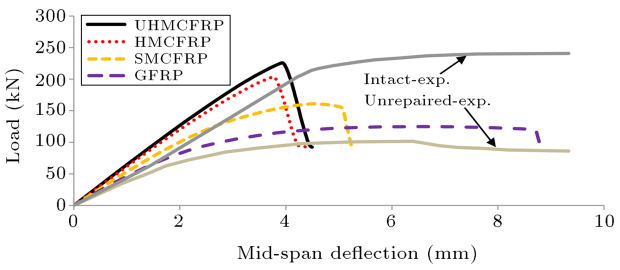

Figure 8. Load-deflection curve of repaired beams with various FRP types.

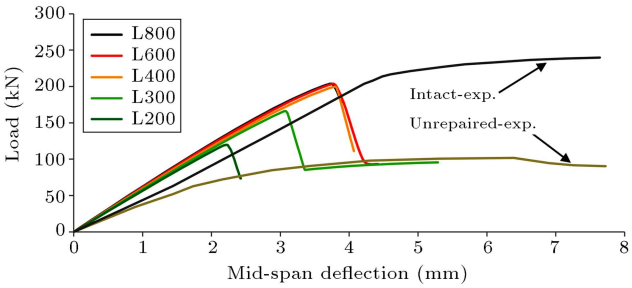

Figure 9. Load-deflection curve of repaired beams with various FRP lengths.

of FRP. This is due to the reality that premature adhesive failure mode tends to occur in more ductile FRP plates than high modulus FRPs. In this case, SMCFRP and HMCFRP plates, for example, led to 69% and 112% increase in load carrying capacity while SMCFRP plate had higher strength than HMCFRP. It should be noted that GFRP and SMCFRP plates utilized only 33% and 35% of their capacity at the time of beam failure, respectively. The GFRP plate, however, is characterized by high ultimate strain, and allows the beam to have more ductility.

4.1.4. Effect of FRP plate length

Another parameter of interest is bond length which is considered to be a variable parameter in an engineering practice which can easily be changed. The longer CFRP plate establishes, the greater area to transmit the shear stress between steel and CFRP. As a result, it causes a growth in bond failure resistance capability of CFRP. As shown in Figure 9, in the case of repaired beam in which the length of CFRP plate was 200 mm (L200), the beam showed a slight increase in load carrying capacity, since the premature debonding occurred when almost half of CFRP capacity was only exploited. Initial stiffness, however, significantly increased because of the transmitting tension stress through CFRP plate at the notch location. In fact, CFRP plate distributes tensile stresses to the bottom steel flange through creating a bridge across the notch. Hence the initial stiffness increased by 40% compared to the unrepaired beam. The repaired beam L300, also, failed due to the complete debonding of CFRP plate when 78% of its capacity was exploited. However, beams L400, L600, and L800 failed when the fiber breakage occurred at the notch location. CFRP plate in L400 experienced a large area of debonding in the vicinity of notch, but finally failed by rupturing of CFRP. When the length of CFRP plate varied from 400 to 800, there was negligible effect on load carrying capacity enhancement. It comes from this reality that stress concentration in the CFRP plate at the notch location does not allow beam to reflect the effect of longer CFRP plate and causes the fiber breakage. Based on this study, it can be concluded that increase

in bond length has a considerable effect on the strength of the joint, but after a certain length, i.e. anchorage length, no increase in the joint strength is observed. As can be seen in Figure 9, the optimum length of FRP plate is obtained when FRP covers 40% of span length, and leads to almost maximum load carrying capacity.

4.2. Effect of adhesive strength

The performance of the interface between FRP and steel is one of the key factors influencing the behavior of the repaired beam. Adhesive strength in the case of attaching CFRP plate to steel surface can have more effect on joint compared to the concrete structures, since unlike RC structures in which debonding failure of the FRP-to-concrete interface mostly occurs in the concrete and a thin layer of concrete is detached, adhesive failure is often predominant in determining bond strength of FRP-to-steel interface. However, the occurrence of cohesive failure within the adhesive layer is valid as long as surface preparation is properly implemented, so that FRP-to-adhesive and the adhesive-to-steel interfaces are strong enough to bear the applied stresses. To demonstrate the effect of adhesive strength, the strengths varying from 4 MPa to 24 MPa were taken into account. It should be noted that there are also commercially available epoxy adhesives for FRP application with greater strength than those of considered in this study, but usually the entire of their nominal strength due to the probable manufacturing defaults as well as the lack of full surface preparation are not exploited.

As shown in Figure 10, an increase of bond strength has considerable effect on the strength of repaired beam when it changes the failure mode from debonding to rupture of CFRP plate. CFRP plates attached using adhesive with strength 4 MPa to 12 MPa (Adh4-Adh12) experienced debonding from steel surface which initiated from notch in early stages of loading and completed when it reached the debonded area which initiated from the end of CFRP plate at further stages of loading. As can be seen in Figure 10, increasing adhesive strength higher than 16 MPa had almost no effect on the global behavior of the repaired

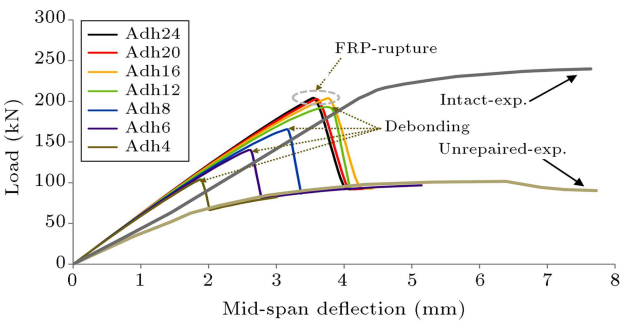

Figure 10. Load-deflection curve of repaired beams with various adhesive strengths.

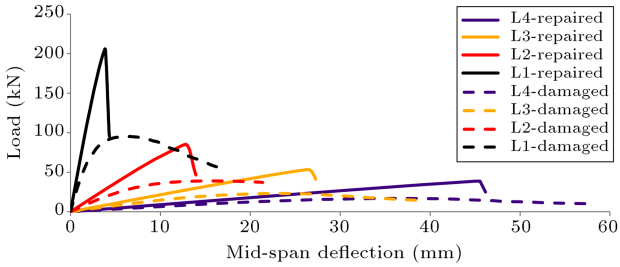

Figure 11. Load-deflection curve of repaired beams with various lengths.

beams. It shows that this parameter can only influence on preventing CFRP from premature debonding failure mode and has negligible effect on the distribution of axial strain in the CFRP plate near the notch location. In other words, 16 MPa is the critical adhesive strength at which the full efficiency of the adhesively bonded plate was attained.

4.3. Effect of steel beam length

In order to have a perspective toward the effect of beam length on efficiency of FRP-repair, four different beam lengths were considered. Figure 11 shows the load-deflection response of repaired beams with the length varying from 1 m to 4 m in which the CFRP plates covered 66% of the free span. This figure indicates that attaching CFRP plate in a constant percent of the free span has almost the same comparative effect on improving the load carrying capacity of various lengths of beams. As shown in this figure, the ultimate strength in all repaired beams improved by about 115% compared to their corresponding damaged beams. Based on this specific study, it can be concluded that in the point of view of the comparative increasing in the load carrying capacity, short-span beams are able to represent the behavior of analogous beams with greater span as long as the instability modes are prevented.

4.4. Effect of strength of steel beam

In order to investigate the effect of the steel strength on the efficiency of CFRP-repair, the steel beams with different yielding stresses, f_y = 200, 250, 300, 350, 400, 450, 500 MPa (called y200 - y500), were adopted. These beams were repaired using HMCFRP plates. The corresponding load-deflection curves are plotted in Figure 12. This shows that the ultimate load increases for higher levels of the steel strength, when yielding stress increases from 200 MPa to 350 MPa. However, it demonstrates a negligible growth in the ultimate load when yielding stress varies from 400 MPa to 500 MPa. In fact, various ultimate loads come from changing in the failure modes of repaired beams. In the case of y200 (i.e. steel beam with yielding stress of 200 MPa), the beam reached its ultimate strength when a large area in the compressive flange, as well as the notch vicinity, entered into plastic regime. Beams y250 and y300

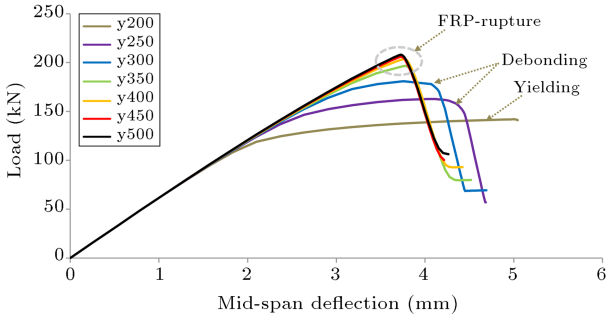

Figure 12. Load-deflection curve of repaired beams with various yielding stresses.

eventually failed by complete debonding of CFRP plate which initiated from notch and grew towards debonded ends of CFRP plate. In spite of the beams which did not experience the full potential load carrying capacity, beams y350, y400, y450, and y500 encountered a brittle failure as a result of fiber breakage in CFRP plate. In this range, increasing the yielding stress caused a reduction in yielded area in the vicinity of crack and, moreover, in the compressive flange, but it had no considerable effect on the whole behavior of the beams. On the other hand, change in yielding stress, obviously, has no influence on initial stiffness of beams, since elastic moduli in the both CFRP plate and steel beams were assumed to be constant.

4.5. Extended studies

4.5.1. Debonding behavior

To have a clear insight into the bond failure mechanism of CFRP-repaired steel beams, the damage indices in the bondline of three beams repaired using CFRP plates with elastic moduli 200 GPa, 400 GPa, and 600 GPa against the distance from the end of CFRP plate are shown in Figure 13. Here, damage index refers to variables that indicate whether a certain damage initiation criterion has been satisfied or not, and a value of 1.0 indicates that the damage initiation criterion has been satisfied. This study showed that in the case of notched beams repaired with adhesively bonding CFRP plate, debonding is often initiated from notch, and as the opening of the mouth of notch is increased, the intermediate debonding propagates toward ends of CFRP plate. Meanwhile, with further increase in the applied load, debonding is also initiated at the ends of CFRP. Schematic damage propagation in steel-FRP interface including intermediate debonding and plate end debonding is shown in Figure 14. The debonded area is finally completed at the areas close to the plate ends, since debonding moves away from the plate ends with lower rate than that from the notch. For example, in the case of repaired beam using CFRP plate with elastic modulus equals to 200 GPa, the debonding development is shown in Figure 15(a)-(d) which demonstrate the debonded area from steel

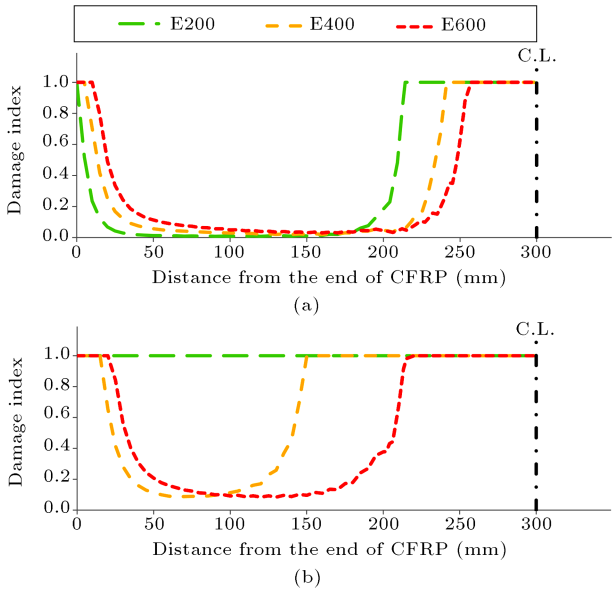

Figure 13. Damage indices in steel-CFRP interface at (a) load 150 kN, and (b) failure load.

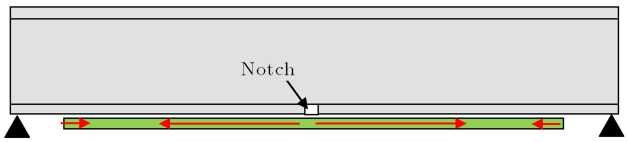

Figure 14. Schematic presentation of damage propagation in CFRP-steel interface.

surface at loads 100 kN, 150 kN, 173 kN, and failure, respectively. These figures clearly show that the development of debonding initiates in a region where the FRP is highly stressed and moves towards the plate ends where the stress in the FRP plate is less. Looking at Figure 13 in which the damage indices in CFRP-steel interface are plotted against the distance from the end of CFRP plates at the load of 150 kN and at the failure load, respectively, it can be found out that in the case of CFRPs with higher modulus of elasticity, there is a higher tendency towards debonding at the end of the CFRP plate while that is less in the vicinity of the crack, when it is compared to CFRP plates with lower elasticity modulus. This phenomenon comes from this reality that the stiffer plate has greater ability to control the mouth opening of the notch than it exists in normal modulus CFRP plates. This study shows that FRPs with higher modulus have more potential to be debonded at the end of plate while its tendency (to debonding) in the vicinity of the crack is less than FRPs with lower modulus.

4.5.2. Rupturing behavior

Figure 16 shows a configuration in which the sectional forces are in equilibrium, where F_F, F_W and F_P are forces carried by compression flange, steel web, and CFRP plate respectively. It shows a situation where

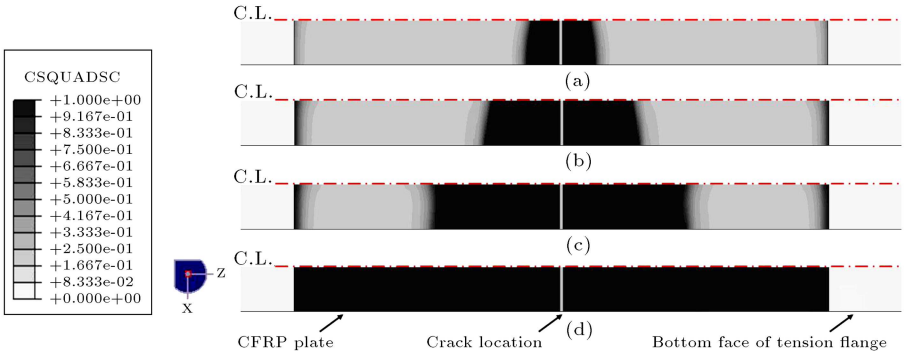

Figure 15. Development of debonding at (a) load 100 kN, (b) load 150 kN, (c) maximum load, (i.e. 173 kN), and (d) failure load.

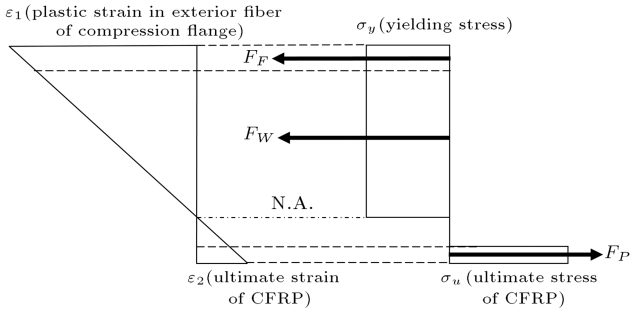

Figure 16. Strain and stress diagram for state of balance between forces carried by steel beam and CFRP plate.

the entire section of the steel beam, at the mid-span, is in post-elastic regime, and the compressive forces carried by steel beam are equal to strength of CFRP plate. This situation is almost analogous to cases that notched steel beam repaired with high modulus FRPs considered in the parametric study. It shows that increasing the thickness of FRP neutral axis would be located in the CFRP plate. Using sectional equilibrium and strain compatibility, the critical thickness which causes decrease in the ultimate strength can be calculated. For example, the critical thickness of CFRP plate for the beam used in the parametric study is 4.13 mm and thicknesses which are thicker than 4.13 mm would not lead to any increase in the ultimate strength of the beam. In this situation, increasing thickness of the CFRP plate would have no effect on enhancing load carrying capacity, since neutral axis would move into CFRP plate so that beam capacity would be decreased. Based on this concept, the repaired beams with CFRP thickness of 4.5 mm and 5 mm showed a reduction in ultimate strength in comparison to the repaired beam with CFRP thickness of 4 mm. That is shown in Figure 7.

5. Conclusion

In this study, a numerical model to investigate the efficiency of CFRP-repair in improving the performance of the notched beams was developed. Then, the validated three-dimensional nonlinear finite element model was employed to achieve the main objective of this study; Particular emphasis on the effect of the dimensions and mechanical properties of the composite and adhesive on the behavior of the notched beams. Based on this study, the following conclusions were drawn:

1. When the strength of CFRP is assumed to be constant, increasing the elastic modulus of CFRP plates leads to an increase in the elastic stiffness of damaged beam, while it does not necessarily enhance the ultimate load of the beam.
2. Increasing the thickness of the CFRP plate up to a critical level leads to an enhance in the load carrying capacity, but thicknesses over this amount makes a reduction in the strength of the beam due to the premature debonding failure mode.
3. The most significant role of the length of the FRP plate is its effect on changing the failure mode. Increasing the length of FRP plate changes the failure mode from debonding to rupturing, and as a result the strength of the beam increases until the optimum length is attained. But any further increase in the bond length has no influence on the beam behavior.
4. GFRP plate has higher ultimate strain than that of other types of FRP, allowing more ductile behavior, but its influence on improving strength and the elastic stiffness was less than the other types of FRP, i.e. CFRP plates. Similarly, it was concluded that although FRP plates with lower elastic modulus tend to debond at the end of plate with lower rate than high modulus FRPs, the intermediate debonding is more profound for the low modulus FRPs compared with the high modulus FRPs.
5. The only effect that can be attributed to the strength of the adhesive layer is its effect on changing the failure mode. For the considered beams, the adhesive with strength higher than 16 MPa maintained the FRP plate in the shear connection with steel surface. However, the amount

of partial debonding in the vicinity of the notch varied through changing the adhesive strength.

6. It was observed that more ductile steel beams in their properties are likely to fail due to the damage progression at the steel-FRP interface, while stiffer steel beams tend to be failed by breakage in the fibers.

7. Partial debonding at the notch location has negligible effect on the beam behavior until it develops and covers the entire interface so that a sudden fall is occurred in the load carrying capacity. The debonding failure mainly depends on the bonding strength and anchorage length. In the case that HM-CFRP plate covered 66% of the span and attached to adhesive strength of16 MPa ensures the prevention of this mode of failure.

8. It was shown that the stiffer CFRP plates, using higher modulus FRPs, tend to fail by rupturing at ultimate load since all the capacity of FRP is exploited. However, it should be considered that using high modulus FRPs brings brittle behavior to repaired beams.

References

1. Yu, Y., Chiew, S.P. and Lee, C.K. "Bond failure of steel beams strengthened with FRP laminates - Part 2: Verification", *Composites: Part B*, **42**, pp. 1122-1134 (2011).

2. Kadhim, M.M.A. "Effect of CFRP plate length strengthening continuous steel beam", *Construction and Building Materials*, **28**, pp. 648-652 (2012).

3. Seleem, M.H., Sharaky, I.A. and Sallam, H.E.M. "Flexural behavior of steel beams strengthened by carbon fiber reinforced polymer plates - Three dimensional finite element simulation", *Materials and Design*, **31**, pp. 1317-1324 (2010).

4. Dawood, M., Sumner, E., Rizkalla, S. and Schnerch, D. "Strengthening steel bridges with new high modulus CFRP materials", in *Third International Conference on Bridge Maintenance, Safety and Management* (IABMAS'06), Portugal (2006).

5. Fam, A., MacDougall, C. and Shaat, A. "Upgrading steel-concrete composite girders and repair of damaged steel beams using bonded CFRP laminates", *Thin-Walled Structures*, **47**, pp. 1122-1135 (2009).

6. Haghani, R. and Al-Emrani, M. "A new design model for adhesive joints used to bond FRP laminates to steel beams - Part A: Background and Theory", *Construction and Building Materials*, **34**, pp. 486-493 (2012).

7. Harries, K.A., Richard, M.J. and Kim, Y.J. "Fatigue behaviour of CFRP retrofitted damaged steel beams", in *Proceedings of 13th International Conference on Structural Faults and Repair*, Edinburgh (2010).

8. Hmidan, A., Kim, Y.J. and Yazdani, S. "CFRP repair of steel beams with various initial crack configurations", *Journal of Composites for Construction ASCE*, **15**, pp. 952-962 (2011).

9. Howard, S.L. "Repair of notched steel beams using ultra-high modulus carbon fibre reinforced polymer", M.Sc. (Eng.) Thesis, Department of Civil Engineering, Queen's University, Kingston, Ont., Canada (2006).

10. Kim, Y.J. and Brunell, G. "Interaction between CFRP-repair and initial damage of wide-flange steel beams subjected to three-point bending", *Composite Structures*, **93**, pp. 1986-1996 (2011).

11. Linghoff, D. and Al-Emrani, M. "Performance of steel beams strengthened with CFRP laminate - Part 2: FE analyses", *Composites: Part B*, **41**, pp. 516-522 (2010).

12. Liu, X., Silva, P.F. and Nanni, A. "Rehabilitation of steel bridge members with FRP composite materials", in *Proc., CCC 2001, Composites in Construction*, pp. 613-617, Porto, Portugal (2001).

13. Tavakkolizadeh, M. and Saadatmanesh, H. "Repair of damaged steel-concrete composite girders using carbon fiber-reinforced polymer sheets", *Journal of Composites for Construction ASCE*, **7**, pp. 311-322 (2003).

14. Kumar, A.M. and Hakeem, S.A. "Optimum design of symmetric composite patch repair to centre cracked metallic sheet", *Comp. Struct.*, **49**, pp. 285-292 (2000).

15. Liu, C.F., Jou, H.S. and Lee, Y.T. "Stress intensity factor of a patched crack", *Int. J. Solid Struct.*, **34**, pp. 1557-1562 (1997).

16. Brighenti, R., Carpinteri, A. and Vantadori, S. "A genetic algorithm applied to optimisation of patch repairs for cracked plates", *Int. J. of Solids and Structures*, **44**, pp. 466-475 (2006).

17. Tsai, G.C. and Shen, S.B. "Fatigue analysis of cracked thick aluminium plate bonded with composite patches", *Compos. Struct.*, **64**, pp. 79-90 (2004).

18. ABAQUS. ABAQUS/standard user's manual. ABAQUS Inc. (2010).

19. ACI, *Building Code Requirements for Structural Concrete (ACI 318-08) and Commentary* (2008).

20. Hashin, Z. "Failure criteria for unidirectional fiber composites", *Journal of Applied Mechanics*, **47**, pp. 329-334 (1980).

21. Davila, C.G., Camanho, P.P. and Rose, C.A. "Failure criteria for FRP laminates", *Journal of Composite Materials*, **39**, pp. 323-345 (2005).

22. Camanho, P.P. and Davila, C.G. "Mixed-mode decohesion finite elements for the simulation of delamination in composite materials", *NASA/TM-2002-211737*, pp. 1-37 (2002).

23. Godat, A., Labossière, P. and Neale, K.W. "Numer-

ical investigation of the parameters influencing the behaviour of FRP shear-strengthened beams", *Construction and Building Materials*, **32**, pp. 90-98 (2012).

Biographies

Mehdi Motaleb received his BS degree in Civil Engineering from Azad University, Tehran South and MS degree in Structural Engineering from Amirkabir University of Technology, Tehran, Iran. He is currently a PhD student at Saint Louis University, USA. His research interests are in the areas of bridges, composite materials, modeling, rehabilitation of structural members using FRP materials, and structural health monitoring.

Mohammad Zaman Kabir is Professor and Chair of Civil and Environmental Engineering Department at Amirkabir University of Technology, Tehran, Iran. He received his BS and MS degrees from Amirkabir University of Technology and his PhD degree from Waterloo University in Canada. His research interests include structural stability, structural analysis using FEM, experimental methods in structural engineering, composite structures, structural optimization, damage detection and rehabilitation of structures.